Published online 21 August 2006 *Nucleic Acids Research, 2006, Vol. 34, No. 16* ***4313–4323***
doi:10.1093/nar/gkl420

IS*911* transpososome assembly as analysed by tethered particle motion

N. Pouget[1,2], C. Turlan[1], N. Destainville[3], L. Salomé[2] and M. Chandler[1,*]

[1]Laboratoire de Microbiologie et Génétique Moléculaire (UMR CNRS 5100), 118 route de Narbonne, 31062 Toulouse cedex, France, [2]Institut de Pharmacologie et Biologie Structurale (UMR CNRS 5089), 205 route de Narbonne 31077 Toulouse cedex, France and [3]Laboratoire de Physique Théorique (UMR CNRS 5152), IRSAMC, Université Paul Sabatier, 118 route de Narbonne, 31062 Toulouse cedex, France

Received March 14, 2006; Revised May 22, 2006; Accepted May 24, 2006

ABSTRACT

Initiation of transposition requires formation of a synaptic complex between both transposon ends and the transposase (Tpase), the enzyme which catalyses DNA cleavage and strand transfer and which ensures transposon mobility. We have used a single-molecule approach, tethered particle motion (TPM), to observe binding of a Tpase derivative, OrfAB[149], amputated for its C-terminal catalytic domain, to DNA molecules carrying one or two IS*911* ends. Binding of OrfAB[149] to a single IS*911* end provoked a small shortening of the DNA. This is consistent with a DNA bend introduced by protein binding to a single end. This was confirmed using a classic gel retardation assay with circularly permuted DNA substrates. When two ends were present on the tethered DNA in their natural, inverted, configuration, Tpase not only provoked the short reduction in length but also generated species with greatly reduce effective length consistent with DNA looping between the ends. Once formed, this 'looped' species was very stable. Kinetic analysis in real-time suggested that passage from the bound unlooped to the looped state could involve another species of intermediate length in which both transposon ends are bound. DNA carrying directly repeated ends also gave rise to the looped species but the level of the intermediate species was significantly enhanced. Its accumulation could reflect a less favourable synapse formation from this configuration than for the inverted ends. This is compatible with a model in which Tpase binds separately to and bends each end (the intermediate species) and protein–protein interactions then lead to synapsis (the looped species).

INTRODUCTION

One of the initial steps in mobilization of transposable genetic elements is binding of the element-specific enzyme, the transposase (Tpase) to each end and their rapprochement into a nucleoprotein complex, the transpososome. Transpososome assembly is a central check point in transposition. In some, and perhaps all, elements, a Tpase molecule bound to one transposon end is programmed to cleave the partner end rather than the end to which it is bound (1–4). A productive synaptic complex must thus be assembled before catalysis can occur. Another characteristic of some transpososomes is an increasing stability as they evolve to a productive complex (2,5,6). This is presumably because of progressive interwrapping of the various protein and DNA components. Synaptic complexes have been observed *in vitro* for several transposable elements including phage Mu (7), IS*10* (Tn*10*) (2), Tn*5* (IS*50*) (8), Tn*7* (9) and IS*911* (10). Although all these elements encode a transposase of the DDE superfamily, and therefore presumably transpose using the same chemistry, their detailed transposition pathways are subtly different (11,12).

IS*911*, a member of the widespread IS*3* family of bacterial insertion sequences, uses a two-step transposition mechanism [see (13,14)]. This entails formation of an autonomous, non-replicative, circular intermediate with abutted right (IRR) and left (IRL) ends, which then undergoes integration. The IS*911* ends participate in two different types of synaptic complex (Figure 1a). Complex A, occurs as one of the first steps in the formation of transposon circles: the pairing of both distant IS ends. This paired end complex (PEC) catalyses single-strand cleavage (hydrolysis) at one IS end and strand transfer to the other (trans-esterification). This leads to a structure in which both ends are retained by a single-strand bridge (Figure 1a) resembling a figure eight when formed on a circular plasmid donor. The closed circular IS copy is generated from this by replication (15) and subsequently undergoes integration into a target DNA molecule using the highly recombinogenic IRR–IRL junction. The final integration event occurs within a second type of complex, synaptic

*To whom correspondence should be addressed. Tel: +33 5 61 33 58 61; Fax: +33 5 61 33 58 58. Email: mike@ibcg.biotoul.fr

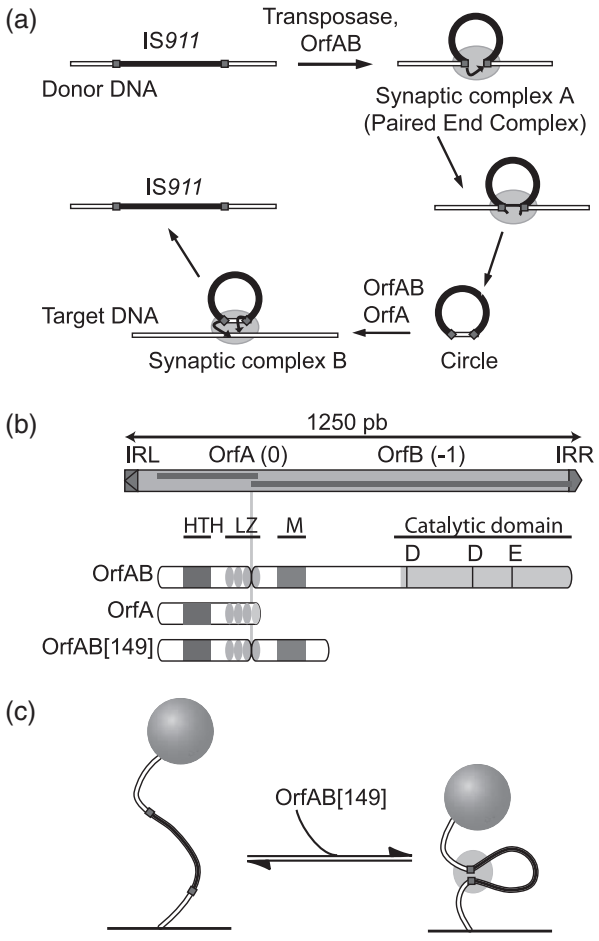

Figure 1. The IS911 transposition cycle, organization of its proteins and single-molecule application. (**a**) Steps in IS911 transposition. IRs: squares; IS*911* sequence: black box; transposase OrfAB: ellipse. The strand cleavage and transfer reactions are indicated by arrows. The transposase stoichiometry in these synaptic complexes is not known. The PEC and circle transposition intermediates are described in the text. (**b**) Organization of IS911 and its protein products (OrfA and the transposase OrfAB). IRs: triangles; open reading frames (orf): dark boxes. The DNA binding domain is composed of a Helix–Turn–Helix motif (HTH, grey box), a Leucine Zipper (LZ, ellipses) and a multimerization domain (M, grey box). The catalytic domain carries a classical DDE motif. The protein used in the assay, OrfAB[149], is a derivative of the OrfAB transposase amputated for the C-terminal catalytic DDE domain. (**c**) Principle of the TPM method. Labelled DNA (white line) with IS*911* sequence (black line) and two IRs (squares) is tethered at one end to a glass surface and a polystyrene bead is attached to the other. Looping of DNA by OrfAB[149] (ellipse) decreases the effective tether length and the amplitude of the bead motion.

complex B, which must be formed between the covalently joined inverted transposon ends and the target DNA.

Formation of synaptic complex A requires the 44 kDa IS*911* transposase, OrfAB, produced as a fusion protein by programmed translational frameshifting between two consecutive and partially overlapping reading frames, *orfA* and *orfB*. OrfAB contains the catalytic site in its C-terminal domain (Figure 1b) and alone, is capable of generating the bridged figure eight form (16).

Synaptic complex A formation has previously been addressed using band shift assays and DNase footprinting (10,17,18). In these studies a derivative of the transposase, OrfAB[149], carrying only the first 149 amino acids (Figure 1b), was used. This derivative is amputated for the catalytic domain and efficiently bound the inverted terminal repeats (IRs) contained in two DNA fragments to generate a PEC (17,18). Increasing the protein concentration also generated a second, faster migrating, species which increased progressively in proportion at the expense of the PEC. This appeared to contain only a single DNA molecule. Protein derivatives shorter than OrfAB[149] and lacking one multimerization region (M; Figure 1b), formed complexes with strikingly modified binding patterns. The results of DNase I footprinting, DNA binding, and *in vivo* recombination measurements suggested a model in which the N-terminal region of OrfAB would bind the subterminal region in a sequence-specific manner anchoring the two IS ends into a PEC. The external region towards the tip of the IR would then contact the catalytic C-terminal transposase domain absent in OrfAB[149] (18).

While these important insights into the assembly of synaptic complex A were generated by population-based molecular approaches, these methods have supplied little information on the dynamics of assembly, the stability of the complexes or the way in which the shorter truncated proteins modify binding. The band shift assay, for example, was not sufficiently temporally sensitive to detect intermediates in PEC formation (18).

We have initiated a single-molecule approach using the tethered particle motion (TPM) method (19) to address synaptic complex assembly and stability. TPM was initially used to observe transcription complexes (20) and subsequently to follow DNA looping mediated by lac repressor (21) and by several restriction enzymes (22). In TPM, the DNA molecule of interest is tethered at one end to a glass surface. The movement of a small bead attached to the other end is visualized by videomicroscopy (Figure 1c). The amplitude of bead movement produced by Brownian motion is a function of effective DNA length.

Here we show that the technique is very sensitive and can apparently detect small curvatures in the DNA induced by OrfAB[149]. Moreover, using DNA molecules carrying two IR sequences with their natural (inverted) orientation and spacing we show that OrfAB[149] generates a species consistent with formation of a loop between the IRs. Once established, these complexes were quite stable. Interestingly they were not only observed with naturally inverted IRs, but could also be detected using substrates with directly repeated IRs. This type of PEC structure would presumably be unable to undergo productive transposition *in vivo*.

TPM also permitted observation of PEC formation in real-time. In contrast to established complexes, the nascent complexes appeared less stable and underwent rapid assembly and disassembly. These experiments also suggested that passage from the protein-bound unlooped to the looped state may involve a species of intermediate length. The data are compatible with a model in which Tpase binds and bends one IR and then the other. Protein–protein interactions could then lead to synapsis generating the looped species.

Compared to classical population-based approaches, TPM offers an enhanced temporal resolution in experiments involving DNA–protein complexes. This has enabled us to detect subtle DNA conformational changes during PEC

formation and provides a basis upon which more detailed studies of transposase-driven synapse formation can be built. In this context, analysis of the behaviour of different transposase derivatives with modified multimerization and DNA binding properties will be particularly important.

MATERIALS AND METHODS

Design and generation of DNA substrates

The length of all but one of the DNA fragments (~2 kb) was chosen to be within the region of best resolution (19). In the case of fragments carrying two IRs the distance between them was close to their natural distance in IS*911* (~1.2 kb). The short 798 bp fragment was designed to approximate the length expected of the longer molecules following synapse of their two IRs. The choice of the pair of DNA fragments with inverted and directly repeated IRs was dictated by the presence of suitable restriction sites permitting inversion of one IR with respect to the other.

DNA substrates were obtained by PCR amplification from plasmid templates with a 5′-digoxigenin-modified forward primer and a 5′-biotin-labelled reversed primer (Eurogentec) as described in Pouget *et al*. (19). The DNA substrates DNA_{R798}, DNA_{R2083}, DNA_{RL2080} were produced using pAPT72 (23) as a template (positions: 1063–1861, 1063–3146, 4625–1861, respectively). The DNA_{2264}, $DNA_{DIR2428}$ and $DNA_{INV2423}$ fragments were produced using pFX288 (positions: 3048–1569), pFX346 (positions: 3130–1651) and pFX347 (positions: 3125–1646), respectively (a gift from F.-X. Barre and C. Pérals). The DNA substrate $DNA_{DIR2428}$ presents a repetition of the segment containing IRR (positions: 619–783 and 1720–1884). The DNA substrate $DNA_{INV2423}$ differs from $DNA_{DIR2428}$ by three fragments in an inverted orientation (positions: 1725–1760, 1764–1797 containing IRR, 1803–1871). The truncated transposase OrfAB[149] was purified from cells carrying pLHT117 (10).

TPM experiments

Experiments were performed using a protocol described in Pouget *et al*. (19). A coverslip flow chamber (30 µl vol) was incubated with the anti-digoxygenin antibody (20 mg/ml; Roche) in phosphate-buffered saline (PBS) for 20 min at 4°C. After washing, the chamber was incubated at 4°C overnight in reaction buffer [20 mM HEPES (pH 7.5), 100 mM KCl, 10 mM $MgCl_2$, 2% glycerol, 2 mM DTT, 10% dimethyl sulfoxide (DMSO), 20 µg/ml BSA, 1 mg/ml dephosphorylated α-casein (Sigma)]. DNA substrates were incubated in the flow chamber for 1 h and labelled with latex beads (0.2 µm diameter neutravidin-labelled microspheres; Molecular Probes). For the majority of experiments, OrfAB[149] was added by flushing the flow chamber with 100 nM OrfAB[149]. For real observations of synapse assembly, 1–2 µl of 6 µM OrfAB[149] were added at one corner of the chamber to let the protein diffused. The tethered beads were visualized by differential interference contrast (DIC) or fluorescence videomicroscopy at a recording rate of 25 frame/s. Bead position was determined on successive images as the spot centroid using a home built image analysis programme (19).

Improved resolution in TPM

In previous analyses, the amplitude of bead motion was measured using either the standard deviation of the abscissa of the bead over successive periods of 4 s (19) or the width of the bead image averaged over 4.3 s (21). Here, we use a more informative method similar to that recently described by van den Broek *et al*. (22). The bead trajectory was acquired at 40 ms intervals. For each 40 ms point, the data were converted into the distance from the barycentre $R = [(x - x_m)^2 + (y - y_m)^2]1/2$ with (x_m, y_m), the coordinate of the barycentre calculated over 2 s. The motion of the bead is the average of R over a 2 s period constituting a sliding window. The length of the window was chosen to satisfy the statistical requirement that it should be much larger than the relaxation time (the characteristic time for the bead to explore its confinement volume). This was determined, from the mean square displacement as a function of time (24,25), to be of the order of 0.1 s for the relevant DNA length range used here. This procedure limits artefacts due to occasional microscope stage drift during image acquisition and permits observation of events occurring at a time scale >2 s thus providing improved temporal resolution.

Measurement of apparent DNA lengths

A calibration curve (data not shown) was established from measurements of the amplitude of bead motion versus known DNA length. The mean amplitude is expressed as the mean of the Gaussian distribution of 'instantaneous' amplitude as calculated above. It was not significantly different from that obtained previously (19). For DNA molecules shorter than 2500 bp, i.e. in the range of interest for this study, the effective length, L, of the molecule can be deduced from the bead amplitude of motion, A, using a linear approximation: $A\ (nm) = 0.079\ L\ (bp) + 16.4$.

Electrophoretic mobility shift assay (EMSA)

DNA substrates used in the permutation assay were produced using pBend2 (26) derivative with IRR (36 pb) cloned at the unique XbaI site. A 1116 pb fragment was first generated by PCR and radiolabelled with dATP-γ32P, and digested with NheI, BbvI, Acc65I or BamHI to produce 163 bp fragment. The binding reactions were performed for 30 min at 30°C with 0.03 µM of the DNA fragment and 0.1 µM OrfAB[149] (a gift from P. Rousseau), in a final volume of 16 µl. Complexes were separated by electrophoresis (12 V/cm, 3 h) in a 5% native polyacrylamide gel (18).

RESULTS

Measurements of DNA length by TPM

In a TPM experiment, a single DNA fragment containing the protein binding sites of interest is anchored to a microscope coverslip by one end and a latex bead is attached to the free end. The amplitude of Brownian movement of the attached bead is related to the effective length of the DNA fragment and is monitored by videomicroscopy (Materials and Methods). Synapsis of two sites on a DNA molecule by the formation of a protein bridge and consequent loop formation will result in a reduction in the effective DNA

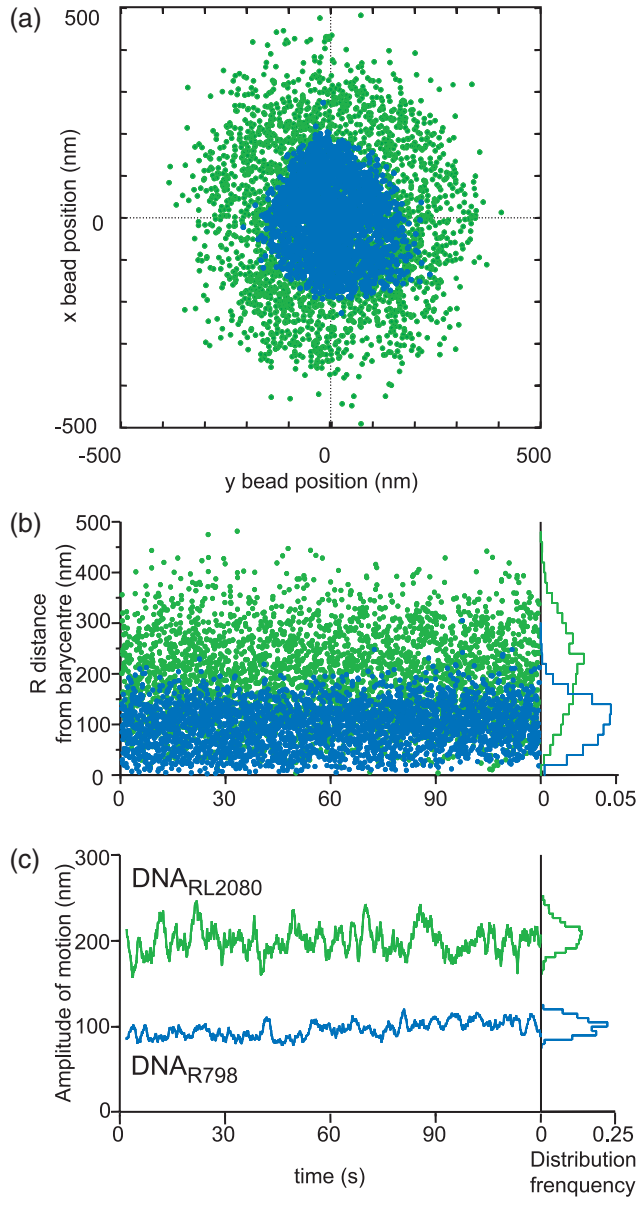

Figure 2. TPM calculation of the amplitude of motion. (**a**) Bead coordinates (x,y). Beads tethered to a glass support by DNA molecules, and therefore undergoing constrained Brownian motion, were tracked for 2 min (blue: $DNAR_{798}$; green: DNA_{RL2080}). (**b**) R positions as function of time. (**c**) Averaged amplitude of motion as a function of time.

length signalled by a decrease in amplitude of bead movement (Figure 1c).

The design of the DNA molecules used is explained in Materials and Methods. A graphic representation of data treatment for two DNA molecules of lengths 2080 and 798 bp (DNA_{RL2080} and DNA_{R798}) is given in Figure 2a–c. The typical raw data are shown in Figure 2a. Bead coordinates *x* and *y* were collected over a period of 2 min. The absence of multiple molecule attachments was assessed by the circularity of the trajectory envelope. The data were converted to a distance, *R*, from the barycentre (Materials and Methods) (Figure 2b) and the amplitude of motion, *A*, was then calculated as a 2 s average of *R*. The plots of *A* as a function of time and the corresponding histograms of frequency distribution (Figure 2c) illustrate the potential of the approach to differentiate DNA molecules of distinct lengths. The mean amplitude is expressed as the mean of the Gaussian distribution with its standard error.

Effects of protein binding to a single IR as revealed by TPM

OrfAB[149] was used in all following experiments. This protein is a derivative of the transposase, OrfAB, amputated for the C-terminal catalytic DDE domain (Figure 1a) and therefore will not promote strand cleavage and transfer. Moreover, it binds IS*911* IRs with higher affinity than the full-length OrfAB (10).

We first analysed the effects of OrfAB[149] binding to DNA with a single IRR using two DNA fragments of 798 bp (DNA_{R798}) and 2083 bp (DNA_{R2083}) each carrying a single IRR located at 238 bp from the free end (Table 1). In the absence of protein, DNA_{R798} exhibited a unimodal distribution with mean amplitude of 106.4 ± 0.2 nm. However, in the presence of OrfAB[149] the distribution was not symmetric (Figure 3a) and was best described by the sum of two populations (Table 1). One had amplitude of 108.1 ± 5.3 nm, similar to that measured in the absence of protein and presumably represented unbound DNA. The second was ∼20 nm smaller with a mean of 89.0 ± 0.6 nm.

Similar results were obtained with DNA_{R2083} (Figure 3b; Table 1) which had a mean length of 198.7 ± 0.2 nm in the absence of protein. In the presence of OrfAB[149], two peaks could be clearly distinguished. Again, the curve was best described as the sum of two populations: (i) with a mean of 201.5 ± 2.1 nm, was indistinguishable from that obtained without protein; (ii) with a mean of 162.4 ± 1.4 nm, was significantly shorter (∼40 nm; Figure 3b).

The reduction in mean amplitude upon addition of protein presumably reflects a reduction in effective length of the DNA as a result of OrfAB[149] binding. To determine whether this was a general property of OrfAB[149] resulting from non-sequence-specific binding or whether it required the specific IR binding site, the experiment was repeated using DNA_{2264}, devoid of IRs. Addition of OrfAB[149] (Table 1 and Figure 3c) had no detectable effect on the apparent length of this DNA fragment (185.2 ± 0.2 nm without protein; 186.3 ± 0.3 nm with protein).

These results demonstrate that OrfAB[149] reduced the apparent DNA length in an IR-dependent manner. The small reduction in length, seen as a reduction in the diameter of the trajectory, probably reflects protein-induced conformational changes, such as DNA bending.

Circular permutation experiments

To examine this further, we used an EMSA to observe the migration of a set of four circularly permuted DNA fragments carrying a single IRR (26). The mobility shift (retardation) of curved or bent DNA is maximal when the bend centre is located at the centre of the DNA fragment [see (27,28)].

This approach was modified to take into account the particular DNA binding and bridging properties of OrfAB[149] observed in EMSA (10,18). DNA fragments of 152 bp

Table 1. DNA fragments used and summary of results (IRR: triangles)

DNA fragments and orientations		Conditions	State	Amplitude of motion ± SE (nm)	Standard deviation (nm)	Relative proportion	Number of beads	Total record duration (min)
End fixed to the bead	End fixed to the glass							
DNA_{R798}	(798 bp)	∅		106.4 ± 0.2	16.6		22	50.9
		OrfAB[149]	Free bound	108.1 ± 5.3	18.4	0.54	31	57.4
				89.0 ± 0.6	11.9	0.46		
DNA_{R2083}	(2083 bp)	∅		198.7 ± 0.2	26.7		29	51.4
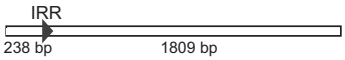		OrfAB[149]	Free bound	201.5 ± 2.1	25.0	0.64	29	53.5
				162.4 ± 1.4	18.2	0.36		
DNA_{2264}	(2264) bp)	∅		185.2 ± 0.2	19.1		22	17.9
		OrfAB[149]	Free	186.3 ± 0.3	21.1		23	19.8
DNA_{RL2080}	(2080 bp)	∅		193.1 ± 0.2	23.0		35	60.8
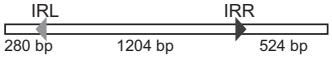		OrfAB[149]	Free bound looped	186.4 ± 1.1	17.4	0.20	44	105.7
				168.4 ± 4.7	39.7	0.51		
				89.5 ± 0.5	15.0	0.29		
$DNA_{INV2423}$	(2423 bp)	∅		194.4 ± 0.2	18.4		45	44.1
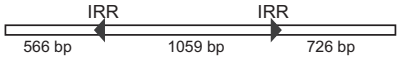		OrfAB[149]	Free bound looped	180.1 ± 2.1	26.1	0.22	50	47.7
				139.1 ± 1.3	8.2	0.04		
				100.5 ± 0.2	17.0	0.72		
$DNA_{DIR2428}$	(2428 bp)	∅		201.5 ± 0.3	23.1		46	50
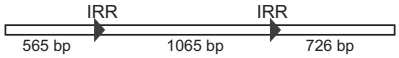		OrfAB[149]	Free bound looped	188.6 ± 0.9	24.8	0.50	47	67.5
				140.9 ± 1.4	11.5	0.10		
				102.7 ± 1.1	18.3	0.40		

Mean values with standard errors (SE) of the amplitudes of motion determined by a Gaussian fit of the distribution for various DNA fragments in absence or in presence of saturating OrfAB[149] concentration. In presence of protein, the table presents the relative proportion for the identified populations.

containing either IRR or IRL and incubated with increasing OrfAB[149] concentrations generated a species (PEC) in which two fragments are bridged by the protein (called complex I). Increasing protein concentration resulted in the progressive appearance of a faster migrating species (complex II) at the expense of complex I. This was interpreted to result from titration of complex I by the additional protein to generate a single DNA fragment bound by protein. Another species (complex III) was occasionally seen. This migrated even further into the gel and its presence depended on the quality of the protein preparation used (the presence or absence of shorter N-terminal fragments). Incubation conditions were chosen here such that complexes with only a single DNA fragment (complex II) were obtained.

To adapt the band shift assay to circular permutation, a fragment of 36 bp, corresponding to the entire IRR, was inserted into the permutation vector pBEND2 (Materials and Methods). We generated an 1116 bp fragment from pBEND2 (Figure 4) using PCR amplification and radiolabelled dATP. This was cleaved with the different restriction enzymes to generate fragments of 163 bp in which the position of the IR was permuted with respect to the fragment end (Figure 4a). The results of the band shift assay are shown in Figure 4b. Although, we chose conditions in which the majority of the retarded species is complex II, we were unable to completely eliminate the occasional appearance of trace amounts (e.g. lane 2) of the slowly migrating PEC (complex I). No complex III was observed with this protein preparation. Uncomplexed substrates migrated at the same positions (data not shown) indicating that no intrinsic bend is present in the 36 bp IRR. The maximum retardation was observed when the IR was located close to the centre of the fragment (lane 2).

These results therefore suggest that OrfAB[149] binding indeed introduces a bend in the DNA, supporting the interpretation that OrfAB[149]-induced DNA shortening observed in the TPM experiments is due to DNA bending. More quantitative studies using DNA fragments carrying specific protein binding sites with known induced angles of curvature are required to explore this more in detail.

DNA loop formation induced by protein binding

To determine whether PEC formation with DNA_{RL2080} could be observed using the TPM technique, the amplitude of bead movement was measured in the presence of OrfAB[149] (Materials and Methods).

Two major peaks were observed in the amplitude distribution shown in Figure 5. That with the smallest amplitude, peak I, was symmetrical and best described as a single population with amplitude of 89.5 ± 0.5 nm. Note that, although this peak appears to include a small shoulder, the fit was not improved by assuming the existence of two populations each with its own Gaussian distribution. We therefore believe this peak to correspond to a single population and the shoulder to be a statistical artefact. Peak II was not symmetrical and was best described by the sum of two populations with amplitudes of 186.4 ± 1.1 nm corresponding to unbound DNA and 168.4 ± 4.7 nm. In view of the results obtained with DNA carrying a single IR (Figure 3, Table 1), this

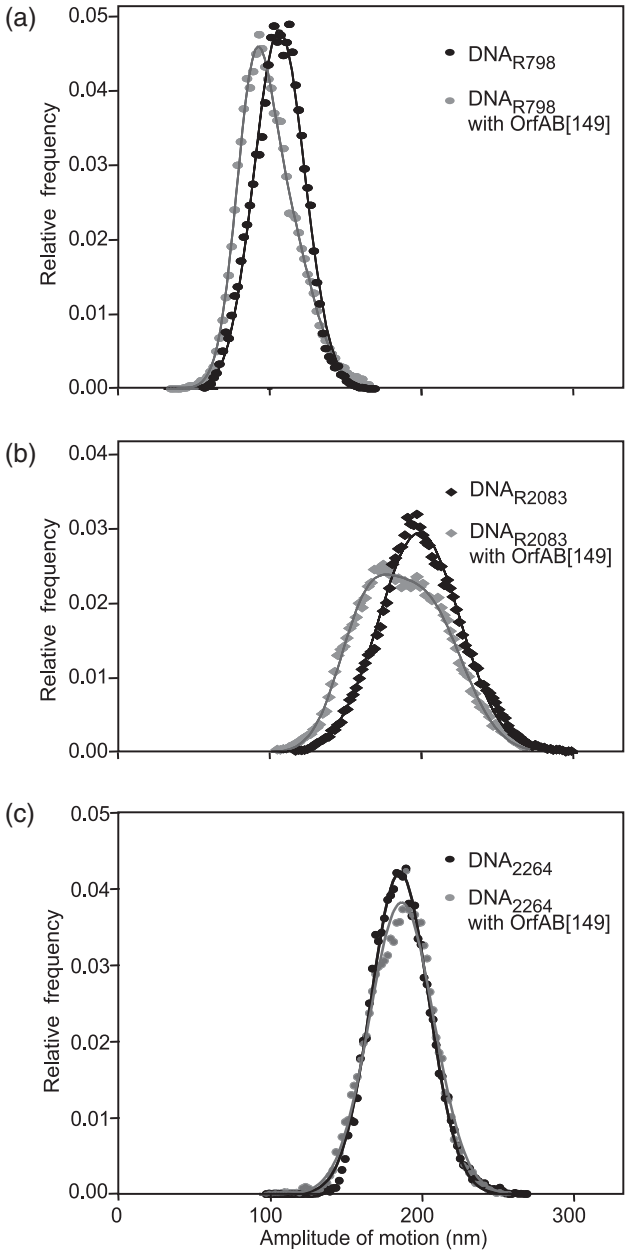

Figure 3. Visualization of protein binding to a single IRR. The relative frequency distribution of amplitude of motion is presented for various DNA fragments in the presence (grey points) or absence (black points) of OrfAB[149] (see also Table 1): (**a**) DNAR$_{798}$: 22 beads analysed without protein, 31 with transposase (**b**) DNAR$_{2083}$: 29 beads analysed without protein, 29 with transposase and (**c**) DNA$_{2264}$: 22 beads analysed without protein, 23 with transposase. The curves show the Gaussian in the absence of OrfAB[149] or double-Gaussian fit for DNA$_{R798}$ and DNA$_{R2083}$ in the presence of OrfAB[149].

shortened species most probably reflects binding of OrfAB[149] to one IR.

Peak I presumably represents DNA molecules in which the two IR copies have been synapsed (PEC). Based on the known DNA sequence, the expected difference in the effective lengths of unbound and looped DNA would be 1276 bp. We found that the difference in mean amplitude of peak I and unbound DNA was 97 nm. This was estimated

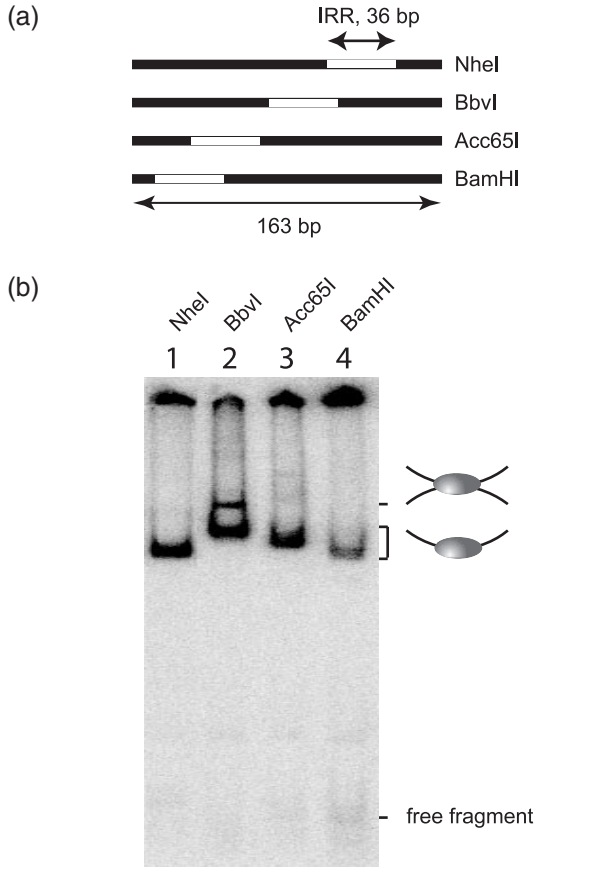

Figure 4. Circular permutation assay. (**a**) Fragments used in the assay (IRR: white boxes). The restrictions enzymes used to generate each fragment are shown on the right. (**b**) EMSA with OrfAB[149]. The restriction enzyme used to generate each fragment is shown above the corresponding lane. The lower mobility complex seen in lane 2, was previously shown to contain two copies of the IRR-carrying fragment (17). The high mobility complex present in each lane corresponds to OrfAB[149] binding to only a single IRR-carrying fragment.

from the standard curve (Materials and Methods) to be 1230 bp. Thus the observed reduction in length is consistent with the formation of a loop.

Kinetics of assembly and stability of the 'looped' complex

To obtain an indication of the kinetics of looped complex formation, a sample of DNA$_{RL2080}$ was exposed to OrfAB[149] and the percentage of long and short molecules was measured over four periods of 15 min at time intervals of 1 h over 3 h. The results, presented in Figure 6 show that over 70% of the molecules observed had already assumed a looped configuration in the first 15 min following addition of the protein. The steady-state was approached after the first hour and reached a value of 80%. The proportion of looped molecules appeared higher than in experiments performed under equilibrium conditions (e.g. Figure 5). Since we were interested in the initial rate of loop formation here, less attention was paid to the presence of elliptical trajectories in the results presented in Figure 6. This could introduce a bias in the relative proportions of looped and unlooped molecules.

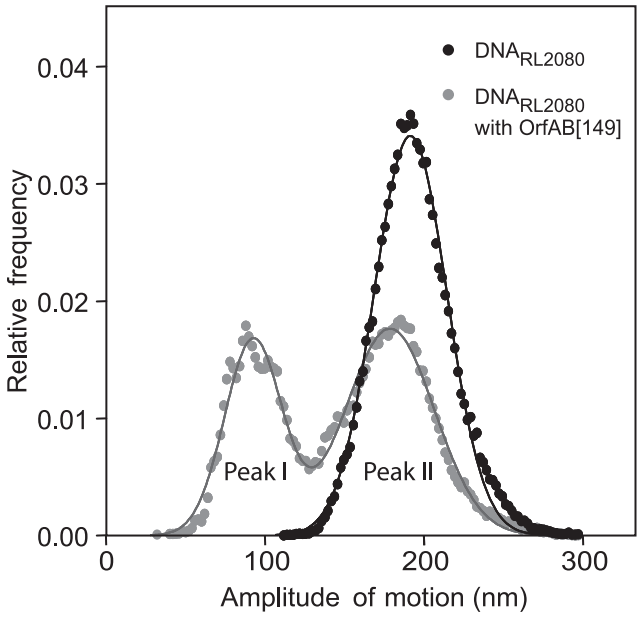

Figure 5. DNA looping in the presence of two IRs. The relative frequency distribution of the amplitude of motion is represented for DNARL2080 with two IRs in the presence (44 beads analysed) or the absence (35 beads analysed) of OrfAB[149] (in grey and black, respectively). The curves show the Gaussian fit of the distributions in the absence of OrfAB[149] or the triple Gaussian fit in the presence of OrfAB[149].

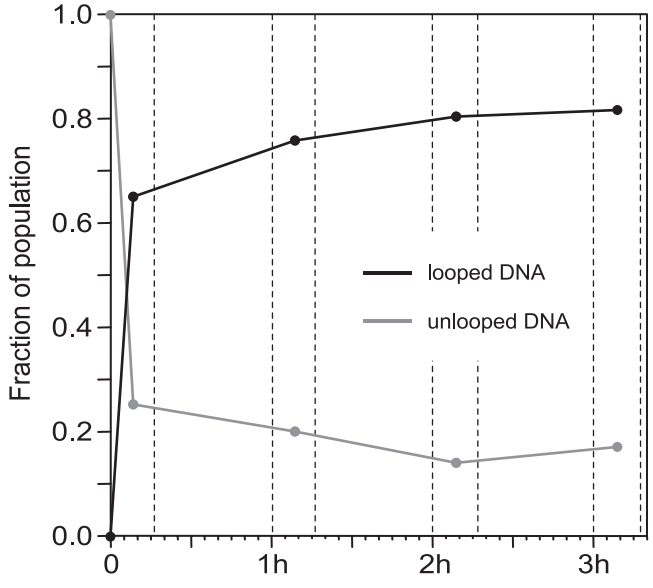

Figure 6. Stability of the looped complex. For DNA$_{RL2080}$ with a saturating concentration of OrfAB[149], the evolution of looped and unlooped fraction of population were observed over a period of 3 h. The proportions of looped and unlooped molecules were estimated over a 15 min period at $T = 0$ min ($n = 158$); $t = 1$ h ($n = 129$); $t = 2$ h ($n = 113$); $t = 3$ h ($n = 99$).

However, the results clearly demonstrate that looped molecules are formed rapidly.

The behaviour of 11 beads showing small amplitude motion after addition of OrfAB[149] was observed for at least 30 min. No disassembly of these complexes to generate extended DNA molecules was detected even for short periods

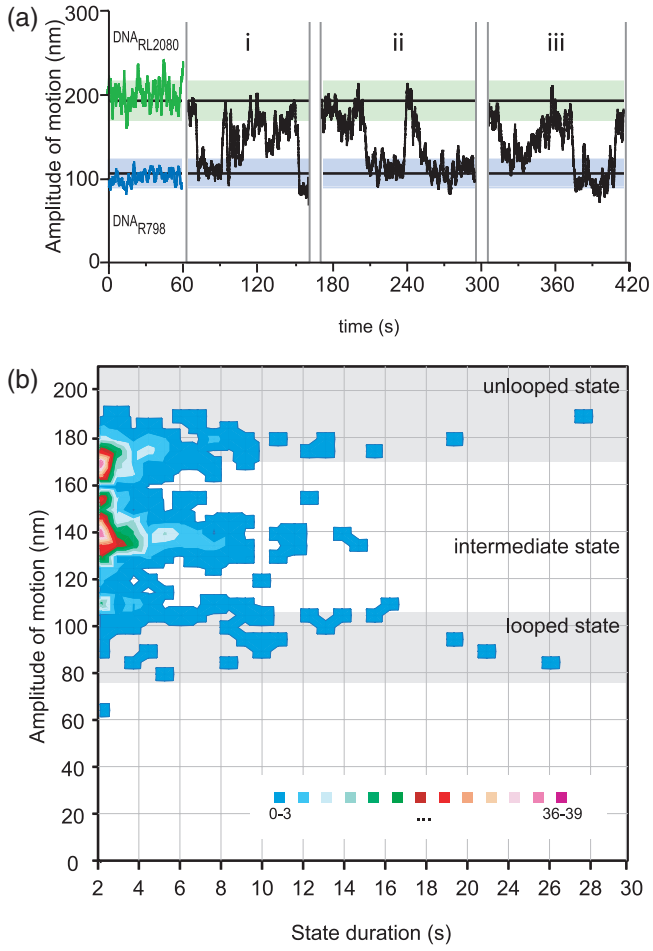

Figure 7. Assembly and disassembly of the synaptic complex in real-time. (**a**) DNA looping by OrfAB[149]. Typical data traces without protein obtained with DNA$_{RL2080}$ (green shading: 193.1 ± 23.0 nm) and DNA$_{R789}$ (blue shading: 106.4 ± 16.6 nm) are shown on the left (0–60 s). Different representative traces of looped and unlooped states are shown on the right (i, ii, ii). Transitions (assembly or disassembly) are clearly not always abrupt, but proceed through intermediate states. (**b**) Histogram of the duration of looped, unlooped, and intermediate states. For each trajectory ($n = 24$), state duration and amplitude were measured. By ploting these two parameters (688 differents states), the intermediate state appears clearly different from the looped and unlooped DNA (grey shade; looped state: 89.5 ± 15.0 nm; unlooped state: 186.4 ± 17.4 nm).

demonstrating that they are quite stable. However, the level of OrfAB[149] in the chamber remained high-throughout for these experiments. To further examine the stability of the complexes, an experiment was performed in which OrfAB[149] was introduced into the microscope cell and allowed to interact for 20 min, a period long enough to approach equilibrium conditions (Figure 6). Excess protein was then flushed from the microscope cell with 20 vol of buffer and 8 looped complexes were observed over 30 min. Again no disassembly could be detected.

We conclude that, once formed, the looped complexes are very stable.

Observation of synapse assembly in real-time

One potentially powerful feature of this technique is that it might be used to observe assembly and disassembly of the

synaptic complex in real-time (21). To test this possibility, tethered beads were identified and tracked within several minutes of introducing OrfAB[149] by diffusion from one corner of the microscope chamber. Several molecules were observed to undergo transitions. Representative traces of the amplitude of movement are presented in Figure 7a. Note that unlooped molecules which undergo transitions to a looped state are consistently shorter than those observed in the absence of protein (Figure 7a, left). This shortening is characteristic of OrfAB[149]-bound DNA (see Figure 3). Transitions of these unlooped molecules to shorter species and vice versa were observed and are consistent with the assembly and disassembly of the synaptic complex. Close scrutiny of the traces showed, however, that they could be quite complex. Transitions often appeared to proceed through complexes with intermediate lengths (between looped and unlooped) and variable duration detected as plateaux on the traces (see Figure 7a). These were identified as periods of restricted amplitude fluctuations flanked by abrupt variations (Materials and Methods). Only unlooped and looped molecules which underwent two transitions over the duration of the experiment (i.e. which were flanked by transitions; e.g. Figure 7a i, ii, ii) were used in the following analysis.

In Figure 7b, the mean amplitude of each plateau was calculated and plotted as a function of its corresponding duration. The results clearly reveal three groups of transient configurations: protein-bound unlooped (which is shorter than substrate DNA without protein), intermediate and looped. None of molecules observed became stabilized at the intermediate length.

These intermediate species might reflect steps during which one protein-bound end is seeking its partner or short-lived species carrying protein-bound to each end.

Synapse with directly repeated IRs

The observation that two correctly oriented (inverted) IRs can form a PEC prompted us to determine whether relative IR orientation plays a role in PEC formation. For this, we compared DNA fragments of 2423 bp carrying two IRR copies as inverted repeats ($DNA_{INV2423}$) and of 2428 bp carrying two IRR copies as direct repeats ($DNA_{DIR2428}$) (Table 1). In both DNA molecules, one IRR is located 726 bp from the DNA end to be anchored to the glass support. The second IR is located at 566 bp from the free end in an inverted orientation ($DNA_{INV2423}$) or 565 bp in a direct orientation ($DNA_{DIR2428}$). The results are shown in Figure 8. Without protein, $DNA_{INV2423}$ (Figure 8a) generated a single peak with an amplitude of 194.4 ± 0.2 nm. Addition of OrfAB[149] generated two major peaks of 180.1 ± 2.1 nm and 100.5 ± 0.2 nm representing unlooped protein-bound DNA and looped DNA, respectively. No 194.4 nm peak was observed although careful scrutiny of the curves obtained for the $DNA_{INV2423}$ substrate (Figure 8a) revealed that the 180.1 ± 2.1 nm peaks included a small shoulder on the right hand side presumably representing unbound DNA. This indicates that the majority of observed DNA molecules had been bound by OrfAB[149]. Since bound and unbound population could not be resolved in this particular case, the mean amplitude is a combination of both populations and this leads to an overestimate of the amplitude of the bound, unlooped DNA.

The 100.5 ± 0.2 nm peaks also carried a small shoulder on the right hand side, which could be resolved and gave a value of 139.1 ± 1.3 nm. This may be the result of OrfAB[149] binding to both IRs in the unlooped DNA since a second DNA bend introduced by binding the second IR should further reduce the amplitude of movement (see Discussion). This population was not detected (or resolved) in the case of DNA_{RL2080}. We also note that the efficiency of loop formation with $DNA_{INV2423}$ was significantly greater than that with DNA_{RL2080} carrying inverted copies of IRR and IRL (Figure 5). These two observations may reflect the proximity of the bead to one IR (280 bp for DNA_{RL2080} and 565 or 566 bp for $DNA_{INV2423}$ and $DNA_{DIR2428}$), which might affect loop formation due to steric hindrance.

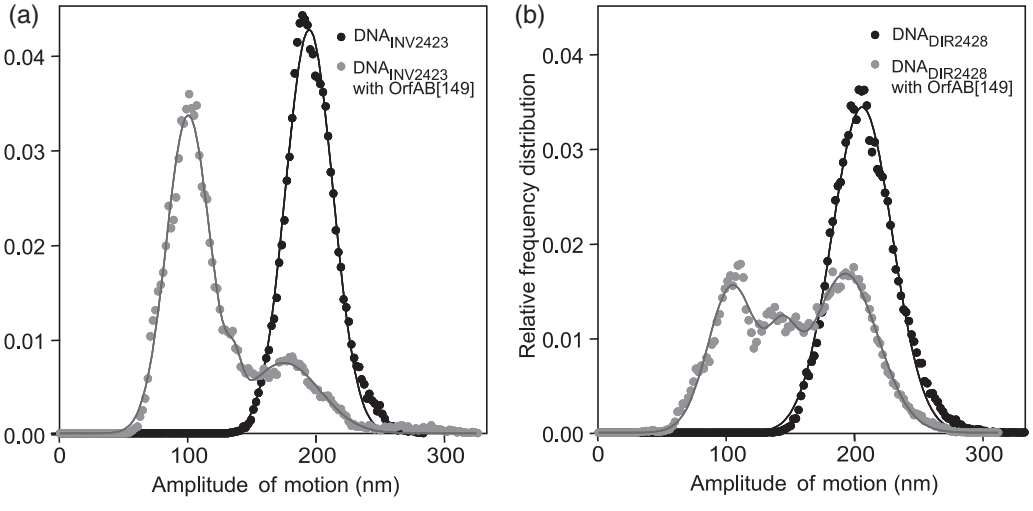

Figure 8. DNA looping in the presence of two IRs in inverted and direct orientations. The relative frequency distribution of the amplitude of motion is shown for (**a**) $DNA_{INV2423}$ with inverted repeated IRR (45 beads analysed in the absence and 50 in the presence of OrfAB[149]). (**b**) DNADIR2428 with directly repeated IRR in the presence (47 beads) or the absence (46 beads) of OrfAB[149] (in grey and black, respectively). The curves show the Gaussian fit or the triple Gaussian fit in the presence of OrfAB[149].

The behaviour of $DNA_{DIR2428}$ (Figure 8b) is different. Although this DNA generated a single peak with an amplitude of 201.5 ± 0.3 nm without protein, it generated three clearly resolvable peaks in the presence of OrfAB[149]. These had amplitudes of 188.6 ± 0.9, 140.9 ± 1.4 and 102.7 ± 1.1 nm. Again the absence of a detectable peak at 201.5 nm suggests that the majority of observed DNA molecule were protein-bound. The 188.6 ± 0.9 nm peak presumably represents non-looped DNA with bound protein while the 102.7 ± 1.1 nm peaks had amplitude expected for looped DNA. The fact that the relative proportion of the looped species was significantly lower for $DNA_{DIR2428}$ compared to $DNA_{INV2423}$ suggests that synapsis of the two directly repeated IRs is less efficient than that of two inverted IRs. The third, intermediate, peaks had amplitude of 140.9 ± 1.4 nm, similar to the population distinguished by the shoulder observed with $DNA_{INV2423}$. This may also represent unlooped DNA with protein-bound to each IR. Its relatively higher abundance (10% versus 4% in the case of the substrate with inverted IRs in this experiment) suggests that it might accumulate at the expense of the looped species. This might be either on the pathway to loop formation or a dead end product.

DISCUSSION

We have demonstrated that TPM can be used to monitor the formation of synaptic or PECs between the ends of the bacterial insertion sequence IS*911*. The method is simple and should be applicable to the study of other transposable elements.

We have used OrfAB[149], a transposase derivative that was chosen as a technical compromise since it was found to bind more readily to the terminal IRs than does the full-length OrfAB protein (10). Although we believe that its binding approximates that of OrfAB, it is possible that it is not identical and that the presence of the C-terminal domain changes the kinetics of binding and PEC formation. Further studies will be needed to improve OrfAB binding either by changes in binding conditions or by generating full-length mutant derivatives with increased binding capacity as has been done in the case of Tn*5* (29).

Detection of changes in DNA conformation

DNA compaction by the DNA bending protein IHF has been previously observed using a similar TPM approach (30). In this case, however, the non-specific binding contribution of IHF appeared to mask the bend introduced by a single IHF dimer on its specific target sequence. However, it was postulated that detection of single binding events requires the use of a short (~10–20 nm) DNA fragment for sufficient resolution (31). Indeed, using a more sophisticated TPM approach these authors revealed that IHF shortened a small DNA fragment carrying a single IHF binding site, consistent with DNA bending. In view of the difficulties experienced in demonstrating IHF-induced bending [known to be >160° (32)], it was therefore unexpected that the simple TPM system with long DNA molecules used in the present study would be sufficiently sensitive to detect small protein-induced DNA bends introduced by OrfAB[149] binding to a single specific site.

The single IR in the fragment (Figure 3) was essential to obtain the small but consistent decrease in apparent length of a DNA fragment in the presence of OrfAB[149]. Results from population-based experiments using EMSA and a set of four circularly permutated DNA fragments in which an IRR copy is located at different distances from the end (Figure 4) support the view that this shortening is due to DNA bending. However, we do not think that we have sufficient data to draw quantitative conclusions about the bend angle. Note that with a single IRR, two molecules with different lengths (DNA_{R798} and DNA_{R2083}) give different amplitude reductions. Therefore within the limits of experimental error, protein binding to a single site can be considered to reduce the amplitude by about 30 nm with an uncertainty of 10 mn.

It will be important to investigate and generalize the experimental relation between DNA amplitude and protein-induced bending using a more defined protein–DNA binding system for which detailed structural and thermodynamic information is available.

Formation and observation of PECs

An additional OrfAB[149]-dependent species was observed if two IR copies were present on the same DNA molecule in an inverted configuration (Figure 5). Its apparent length was consistent with the formation of an IR–IR synapse. Once formed, this appeared quite stable over periods of at least 30 min even if excess protein was removed by flushing the chamber (data not shown).

Kinetic analysis showed that loop formation occurred relatively rapidly (Figure 6): most of the complexes had been formed within the first 15 min. Moreover, results obtained from visualization of molecules undergoing transitions following injection of OrfAB[149] into the chamber (Figure 7a) indicated that assembly of the nascent complexes did not necessarily occur in a single step. Before such complexes were established, steps of assembly and disassembly could be observed. These were often accompanied by the formation of molecules of intermediate length (Figure 7a and b). These observations suggest that complexes pass through a metastable state. The nature of these metastable complexes remains to be determined.

Complex formation with directly repeated IRs

To address some of these questions, we analysed the behaviour of DNA molecules with directly repeated IRs. In previous analyses (33) where reactions between both inverted and directly repeated IRs were in competition, we were unable to detect cleavage or strand transfer reactions between the directly repeated IRs. This presumably resulted from inherently less favourable PEC formation between such ends due to an energetic cost of, e.g. introducing an additional twist when forming a loop. Consistent with this, PEC formation was indeed observed with directly repeated IRs using the TPM approach but with lower efficiency than when using a substrate with inverted IRs (Figure 8).

In addition to the looped and unlooped molecules observed with the substrate carrying directly repeated IRR copies, a pronounced peak of intermediate length was observed (Figure 8b). A species with similar amplitude was observed

for the substrate with inverted IRRs (Figure 8a) as a shoulder to the right of the looped DNA population. These may correspond to the transitory intermediate state observed during looping of a substrate with inverted IRs (Figure 7).

The intermediate species: a plausible model

The intermediate species seen in Figure 7b and those observed in equilibrium conditions (Figure 8 and Table 1) are probably the same type of complex. These could reflect the formation of loops of intermediate length by an OrfAB[149] complex bound to one end while searching for the other. It is possible that additional weak OrfAB[149] binding sites are present between the IRs. However, we were unable to identify sequences with significant similarities to the defined OrfAB[149] binding sites [data not shown, (18)]. In addition, such intermediate states were not observed using substrates with a single IR.

A second and simpler explanation is that these species represent DNA molecules with OrfAB[149] bound to both IRs. This interpretation stems from the DNA length reduction provoked by OrfAB[149] binding to the IRs (Figure 3). In contrast to EMSA, in which one bend can cancel the effect of another depending on relative position and geometry (27,28), in TPM (a situation where one end of the DNA molecule is anchored), bends should have a cumulative effect. Doubly bound DNA would therefore be expected to undergo a larger reduction in amplitude than that observed for binding to a single IR.

Such doubly bound species might represent complexes on the pathway to synapse formation or non-productive complexes unable to undergo synapsis. We do not yet know how both ends of IS*911* find each other to form the synaptic complex: whether OrfAB[149] binds to a single end as a multimer, which must then find and bind the second end, or whether it binds both ends and synapsis is driven by protein–protein interactions.

In the experiments shown in Figure 7, only molecules actually undergoing transitions were analysed. These should therefore have protein already bound. This inference is supported by the observation that the 'unlooped' molecules were shorter than the protein-free DNA (Figure 7a). It is probable that only a single IR is occupied in these molecules. The further reduction in length which occurs in the intermediate states could represent occupation of the second IR. If these are complexes on the pathway to synapsis, they might then rapidly evolve into the looped structure by interaction between the OrfAB[149] molecules bound to each end, or disassemble into the singly bound or unbound DNA molecule. Although the molecules were observed for only a short period (mean period of 4 min), of the 17 analysed, 5 went on to form looped complexes from the intermediate state. The remaining 11 appeared to oscillate between the intermediate state and the singly bound state. Therefore while all molecules in an intermediate state do not necessarily give rise to looped molecules over our period of observation, all looped molecules identified had passed through the intermediate state.

The presumed doubly bound molecules were not obvious in all equilibrium studies (see Figure 5). This is either because they represent only a small fraction of bound molecules or because they are confounded with the looped population. They have never been detected in EMSA studies where no pre-PEC intermediates have as yet been observed (10).

These results are consistent with models, such as those proposed for Tn*5* (8), mariner elements (34) and, with experimental support, for retroviral IN activity (35,36). Here transposase molecules are proposed to bind to each end of the transposon separately and synapsis then occurs by interaction between these bound transposase molecules.

This model could also explain the results obtained with the pair of substrates carrying the inverted and directly repeated IRRs (Figure 8). We assume that the shoulder observed on the right of the looped population peak (Figure 8a) with the inverted IR substrate and the pronounced additional peak found with the directly repeated IR substrates are both doubly bound complexes. Generating a PEC with directly repeated IRs might introduce specific constraints not present with the inverted IR substrate: e.g. the introduction of a crossing between the IRs to accommodate their docking. Under these circumstances, a doubly bound DNA molecule with directly repeated IRs would face an energy barrier, not encountered by the inverted IR substrate, in forming a PEC. This would be expected to be accompanied by an increase in the doubly bound intermediate as observed.

The TPM technique is clearly applicable to fine scale analysis of synapsis during transposition. It has revealed several properties of IS*911* synaptic complex formation, which are not detectable by traditional procedures (complex formation in real-time; transient intermediates) and others which are (protein-induced DNA curvature). TPM will be a powerful tool for investigating the importance of multimerization in complex formation by using available mutants defective in this process. The results obtained with OrfAB[149] have paved the way for analysis of PEC formation by the entire OrfAB transposase and, coupled with fluorescence detection, will be used to investigate steps downstream from synapse formation, such as cleavage and strand transfer reactions, and the role of the IS*911* regulatory protein, OrfA.

ACKNOWLEDGEMENTS

The authors would like to thank A. Martinez and D. Icard for performing some of the initial experiments, F-.X. Barre and C. Pérals for the gift of plasmid DNA, P. Rousseau for the gift of OrfAB[149] and for advice in the permutation experiments. We would also like to thank J-F. Allemand and V. Croquette for helpful discussions. N.P. was supported by a doctoral grant from the French Ministry of Education and Research and from the Association pour la Recherche contre le Cancer (ARC). The Chandler, Salomé and Destainville labs were funded by the CNRS. Funding to pay the Open Access publication charges for this article was provided by the CNRS.

Conflict of interest statement. None declared.

REFERENCES

1. Naumann,T.A. and Reznikoff,W.S. (2000) Trans catalysis in Tn5 transposition. *Proc. Natl Acad. Sci. USA*, **97**, 8944–8949.
2. Sakai,J., Chalmers,R.M. and Kleckner,N. (1995) Identification and characterization of a pre-cleavage synaptic complex that is an early intermediate in Tn10 transposition. *EMBO J.*, **14**, 4374–4383.

3. Williams,T.L., Jackson,E.L., Carritte,A. and Baker,T.A. (1999) Organization and dynamics of the Mu transpososome: recombination by communication between two active sites. *Genes Dev.*, **13**, 2725–2737.
4. Swanson,P.C. (2001) The DDE motif in RAG-1 is contributed in trans to a single active site that catalyzes the nicking and transesterification steps of V(D)J recombination. *Mol. Cell. Biol.*, **21**, 449–458.
5. Savilahti,H., Rice,P.A. and Mizuuchi,K. (1995) The phage Mu transpososome core: DNA requirements for assembly and function. *EMBO J.*, **14**, 4893–4903.
6. Surette,M.G., Buch,S.J. and Chaconas,G. (1987) Transpososomes: stable protein–DNA complexes involved in the *in vitro* transposition of bacteriophage Mu DNA. *Cell*, **49**, 253–262.
7. Mizuuchi,M., Baker,T.A. and Mizuuchi,K. (1992) Assembly of the active form of the transposase-Mu DNA complex: a critical control point in Mu transposition. *Cell*, **70**, 303–311.
8. Bhasin,A., Goryshin,I.Y., Steiniger-White,M., York,D. and Reznikoff,W.S. (2000) Characterization of a Tn5 pre-cleavage synaptic complex. *J. Mol. Biol.*, **302**, 49–63.
9. Skelding,Z., Sarnovsky,R. and Craig,N.L. (2002) Formation of a nucleoprotein complex containing Tn7 and its target DNA regulates transposition initiation. *EMBO J.*, **21**, 3494–3504.
10. Haren,L., Polard,P., Ton-Hoang,B. and Chandler,M. (1998) Multiple oligomerisation domains in the IS911 transposase: a leucine zipper motif is essential for activity. *J. Mol. Biol.*, **283**, 29–41.
11. Turlan,C. and Chandler,M. (2000) Playing second fiddle: second-strand processing and liberation of transposable elements from donor DNA. *Trends Microbiol.*, **8**, 268–274.
12. Curcio,M.J. and Derbyshire,K.M. (2003) The outs and ins of transposition: from mu to kangaroo. *Nature Rev. Mol. Cell. Biol.*, **4**, 865–877.
13. Rousseau,P., Normand,C., Loot,C., Turlan,C., Alazard,R., Duval-Valentin,G. and Chandler,M. (2002) Transposition of IS911. In Craig,N.L., Craigie,R., Gellert,M. and Lambowitz,A.M. (eds), *Mobile DNA II*. American Society for Microbiology, Washington,D.C.
14. Ton-Hoang,B., Polard,P., Haren,L., Turlan,C. and Chandler,M. (1999) IS911 transposon circles give rise to linear forms that can undergo integration *in vitro*. *Mol. Microbiol.*, **32**, 617–627.
15. Duval-Valentin,G., Marty-Cointin,B. and Chandler,M. (2004) Requirement of IS911 replication before integration defines a new bacterial transposition pathway. *EMBO J.*, **23**, 3897–3906.
16. Polard,P. and Chandler,M. (1995) An *in vivo* transposase-catalyzed single-stranded DNA circularization reaction. *Genes Dev.*, **9**, 2846–2858.
17. Haren,L., Normand,C., Polard,P., Alazard,R. and Chandler,M. (2000) IS911 transposition is regulated by protein–protein interactions via a leucine zipper motif. *J. Mol. Biol.*, **296**, 757–768.
18. Normand,C., Duval-Valentin,G., Haren,L. and Chandler,M. (2001) The terminal inverted repeats of IS911: requirements for synaptic complex assembly and activity. *J. Mol. Biol.*, **308**, 853–871.
19. Pouget,N., Dennis,C., Turlan,C., Grigoriev,M., Chandler,M. and Salome,L. (2004) Single-particle tracking for DNA tether length monitoring. *Nucleic Acids Res.*, **32**, e73.
20. Schafer,D.A., Gelles,J., Sheetz,M.P. and Landick,R. (1991) Transcription by single molecules of RNA polymerase observed by light microscopy. *Nature*, **352**, 444–448.
21. Finzi,L. and Gelles,J. (1995) Measurement of lactose repressor-mediated loop formation and breakdown in single DNA molecules. *Science*, **267**, 378–380.
22. van den Broek,B., Vanzi,F., Normanno,D., Pavone,F.S. and Wuite,G.J. (2006) Real-time observation of DNA looping dynamics of Type IIE restriction enzymes NaeI and NarI. *Nucleic Acids Res.*, **34**, 167–174.
23. Polard,P., Prere,M.F., Fayet,O. and Chandler,M. (1992) Transposase-induced excision and circularization of the bacterial insertion sequence IS911. *EMBO J.*, **11**, 5079–5090.
24. Qian,H. and Elson,E.L. (1999) Quantitative study of polymer conformation and dynamics by single-particle tracking. *Biophys. J.*, **76**, 1598–1605.
25. Goshen,E., Zhao,W.Z., Carmon,G., Rosen,S., Granek,R. and Feingold,M. (2005) Relaxation dynamics of a single DNA molecule. *Phys. Rev. E Stat. Nonlin. Soft Matter Phys.*, **71**.
26. Kim,J., Zwieb,C., Wu,C. and Adhya,S. (1989) Bending of DNA by gene-regulatory proteins: construction and use of a DNA bending vector. *Gene*, **85**, 15–23.
27. Lane,D., Prentki,P. and Chandler,M. (1992) Use of gel retardation to analyze protein–nucleic acid interactions. *Microbiol. Rev.*, **56**, 509–528.
28. Harrington,R.E. (1993) Studies of DNA bending and flexibility using gel electrophoresis. *Electrophoresis*, **14**, 732–746.
29. Steiniger-White,M., Rayment,I. and Reznikoff,W.S. (2004) Structure/function insights into Tn5 transposition. *Curr. Opin. Struct. Biol.*, **14**, 50–57.
30. Ali,B.M., Amit,R., Braslavsky,I., Oppenheim,A.B., Gileadi,O. and Stavans,J. (2001) Compaction of single DNA molecules induced by binding of integration host factor (IHF). *Proc. Natl Acad. Sci. USA*, **98**, 10658–10663.
31. Dixit,S., Singh-Zocchi,M., Hanne,J. and Zocchi,G. (2005) Mechanics of binding of a single integration-host-factor protein to DNA. *Phys. Rev. Lett*, **94**, 118101.
32. Rice,P.A., Yang,S., Mizuuchi,K. and Nash,H.A. (1996) Crystal structure of an IHF-DNA complex: a protein-induced DNA U-turn. *Cell*, **87**, 1295–1306.
33. Turlan,C., Ton-Hoang,B. and Chandler,M. (2000) The role of tandem IS dimers in IS911 transposition. *Mol. Microbiol.*, **35**, 1312–1325.
34. Auge-Gouillou,C., Brillet,B., Hamelin,M.H. and Bigot,Y. (2005) Assembly of the mariner Mos1 synaptic complex. *Mol. Cell. Biol.*, **25**, 2861–2870.
35. Faure,A., Calmels,C., Desjobert,C., Castroviejo,M., Caumont-Sarcos,A., Tarrago-Litvak,L., Litvak,S. and Parissi,V. (2005) HIV-1 integrase crosslinked oligomers are active *in vitro*. *Nucleic Acids Res.*, **33**, 977–986.
36. Li,M. and Craigie,R. (2005) Processing of viral DNA ends channels the HIV-1 integration reaction to concerted integration. *J. Biol. Chem.*, **280**, 29334–29339.